PHYSICAL REVIEW A VOLUME 5, NUMBER 1 JANUARY 1972

Effect of a Magnetic Field on the Diffusion of an Electron-Hole Plasma in Germanium†

Mark N. Gurnee
Division of Engineering, Brown University, Providence, Rhode Island 02912

and

William M. Hooke
Plasma Physics Laboratory, Princeton University, Princeton, New Jersey 08540

and

George J. Goldsmith
Department of Physics, Boston College, Chestnut Hill, Massachusetts 02167

and

Maxwell H. Brennan
School of Physical Sciences, Flinders University, Bedford Park, 5A 5042 *Australia*
(Received 4 March 1971)

The diffusion of an optically injected electron-hole plasma parallel and perpendicular to an applied magnetic field has been studied in germanium. The density gradient within the crystal has been measured directly by an infrared-beam-absorption technique. Diffusion measurements made parallel to the magnetic field are adequately explained by the theory. For values of $\omega_c\tau > 3.5$ (where ω_c is the electron cyclotron frequency and τ is the electron scattering time with the lattice), the diffusion across the magnetic field is more rapid than that predicted by a theory that takes into account the anisotropic magnetoconductive properties of germanium. If we express the observed diffusion coefficient as the sum of the computed collisional coefficient plus a term D_{excess} representing the additional diffusion, we find that at the largest achievable values of $\omega_c\tau$, D_{excess} is within a factor of 2 of the Bohm value $kT/16eB$ cm^2 sec^{-1}.

I. INTRODUCTION

A great deal of experimental and theoretical work has been devoted to the problem of the diffusion of a gaseous plasma across a magnetic field. The diffusion rate is known to be bounded on the lower side by collisional diffusion; however, many experiments have yielded a diffusion rate much greater than this lower limit. This "anomalous" diffusion has been seen in both fully and partially ionized plasmas.[1–6]

In this paper we study the diffusion of an electron-hole plasma in a semiconductor. For these experiments the dominant collision process is between the charged particles and the crystal lattice, rather than between the electrons and the holes. Therefore, the semiconductor plasma is more closely analogous to the partially rather than the fully ionized plasma.

In a comparison of the two types of plasma, an important parameter is the product $\omega_c\tau$, where ω_c is the cyclotron frequency and τ is the time interval between collisions with the lattice in the semiconductor plasma and the neutral atoms in the gaseous plasma. For $\omega_c\tau < 1$, diffusion in gaseous plasmas has been seen to be collisional, while for $\omega_c\tau > 1$, the diffusion in nearly all gaseous-plasma experiments is much greater than collisional and varies inversely with the first power of the magnetic field, as Bohm predicted.[4] In terms more familiar to solid-state workers, the quantity $\omega_c\tau = \mu B$, where μ is the carrier mobility. Values of $\mu B > 1$ are readily attainable in semiconductor crystals, so it is natural to study cross-field diffusion in these solid-state systems.

The idea of studying plasma-diffusion effects in semiconductors is not new. Ancker-Johnson and Berg have studied the effect of various magnetic field configurations on plasma loss in a semiconductor.[7] They showed that certain field geometries enhanced the lifetime of a plasma that was electrically injected into a semiconductor. However, they did not measure the diffusion coefficient itself, and in fact there has been no direct measurement, in a semiconductor, of the variation of the diffusion coefficient with the magnetic field.

To measure the diffusion coefficient of the electron-hole plasma directly, a method is needed to measure the plasma density within the crystal. We have developed a plasma-density probe that is based on the absorption of a laser beam by the plasma. The technique is an extension of work by Harrick, who used a monochromator as a source of infrared radiation, and measured the spatial

variation of electron density injected across a p-n junction by measuring the free-carrier absorption.[8] Ancker-Johnson and co-workers have used a CO_2 laser as an infrared source, and measured plasma density of the pinch in InSb by measuring free-carrier absorption.[9] Slusher *et al.* have used a 17-μ Ne laser to measure the spatial variation of an electron-hole plasma injected into InSb.[10]

We used a helium-neon laser for our plasma-density measurement. This laser is an intense source of infrared radiation, and the helium-neon laser line at 3.39 μ corresponds almost exactly to a strong absorption peak in germanium, due to an interband hole transition. These two factors make our technique well suited to the measurement of plasma density within the crystal.

Germanium was used as the semiconductor supporting the electron-hole plasma because its electrical properties are well known, and because the diffusion lengths are large enough to be easily resolvable by the density-measuring system. Two geometries were used: a rectangular one and a cylindrical one. The electron-hole plasma was optically injected into the sample by strongly absorbed light at the surface; it diffused into the sample, where the electrons and holes recombined. The combination of diffusion and recombination led to a plasma with a density gradient directed toward the sample surface, with an e-folding length equal to the square root of the diffusion coefficient times the recombination lifetime $L = (D_\perp \tau_r)^{1/2}$. A magnetic field was applied either parallel or perpendicular to the density gradient. With the magnetic field perpendicular to the density gradient, a current flowed perpendicular to both the magnetic field and the density gradient. For the rectangular sample, continuity of this current was achieved by electrical contacts at the ends of the sample and an external circuit. For the cylindrical sample, continuity of the current was maintained entirely within the sample. Measurement of the diffusion length as a function of the magnetic field allowed determination of the variation of the diffusion coefficient with the magnetic field.

The rectangular configuration is equivalent to one that has been used for many years in the study of the photoelectromagnetic (PEM) effect in semiconductors.[11,12] The PEM effect allows the measurement of very short excess carrier lifetimes, under the assumption that the diffusion coefficient is related to the mobility by Einstein's relation. Then the variation of the short-circuit current flowing transverse to both the magnetic field and the density gradient with magnetic field may be related to the mobility and lifetime of the carriers.

The experiment with cylindrical geometry is closely related to that used in measuring the Corbino magnetoresistance in semiconductors.[13] However, in the diffusion experiments we are studying a nonequilibrium concentration of electrons and holes, while for magnetoresistance measurements the effect of the magnetic field on equilibrium electrons or holes is measured.

Our experimental results are compared with a theory derived along familiar lines to describe galvanomagnetic effects in germanium. The starting point of the calculations is the Boltzmann equation. Integration of that equation over d^3k immediately yields the continuity equation. The equation of motion for the plasma carriers follows from a linearized solution of the Boltzmann equation. The effects of anisotropic effective masses of electrons and holes is taken into account. The final result is a prediction of the variation of the plasma ambipolar diffusion coefficient as a function of the applied magnetic field, which is compared with the experimental results.

II. THEORY

To describe the behavior of electrons and holes in a solid-state plasma the effective mass approximation is used. This approximation effectively reduces the complex problem of electrons in a periodic lattice and an additional perturbing potential (the external fields) to a problem much like that of free electrons in the perturbing potentials. The only change is that the free-electron mass is replaced with a "reduced" mass, which may be anisotropic in space.

The Boltzmann equation is written in the form

$$\frac{\partial f}{\partial t} + \frac{\vec{\nabla}_k \epsilon}{\hbar} \cdot \vec{\nabla}_r f + \frac{q}{\hbar}\left(\vec{E} + \frac{\vec{\nabla}_k \epsilon}{\hbar} \times \vec{B}\right) \cdot \vec{\nabla}_k f = \left.\frac{\partial f}{\partial t}\right|_{\text{coll}} + \left.\frac{\partial f}{\partial t}\right|_{\text{recomb}} .$$

Integrating this equation over d^3k, and noting that collisions conserve particles, yields the continuity equation for each species:

$$\frac{\partial n}{\partial t} + \vec{\nabla} \cdot n\vec{v} = \left.\frac{\partial n}{\partial t}\right|_{\text{recomb}} .$$

The recombination term is taken to be of the one-body form $(\partial n/\partial t)_{\text{recomb}} = -(n - n_0)/\tau_r$, where n_0 is the equilibrium carrier density. This form will be shown to be valid by our experimental results.

The equation of motion is derived from a solution of the linearized Boltzmann equation, obtained by writing $f = f_m(\epsilon)\, n(r) + f_1(\vec{k})$, where $f_m(\epsilon)$ is Maxwellian and f_1 is to include linear effects of the fields and gradients.

The perturbation in the distribution function, f_1, is assumed to be small compared with $f_0 = f_m(\epsilon) n(r)$. After substitution of this expression for the distribution function into the Boltzmann equation, re-

grouping terms, and neglecting all second-order terms, we get

$$-\frac{nq}{m}\frac{\partial f_m}{\partial \epsilon}\vec{F}\cdot\vec{\nabla}_k\epsilon=\frac{f_1}{\tau}+\frac{q}{\hbar^2}(\vec{\nabla}_k\epsilon)\times\vec{B}\cdot\vec{\nabla}_k f_1\,, \quad (1)$$

where $\vec{F}=\vec{E}+kT\vec{\nabla}n/nq$ is a generalized force including electric fields and density gradients.

The collision term has been written in the relaxation form $(\partial f/\partial t)_{coll}=-(f-f_0)/\tau$, valid for acoustic phonon scattering. Since we are looking for a stationary solution we have set $\partial f/\partial t=0$. The time scale of recombination is very much longer than that of scattering, so the recombination term in the equation of motion may be neglected. For our purposes the general solution is expressed in the integrated form

$$\vec{\Gamma}=n\vec{v}=n\int f_1\frac{\vec{\nabla}_k\epsilon}{h}\,d^3k\equiv n\overleftrightarrow{U}\cdot\vec{E}\,,$$

where $\overleftrightarrow{U}$ is the magnetic-field-dependent mobility tensor. The solution of this equation depends on the form of $\epsilon(\vec{k})$, the constant energy surface of the holes or electrons in germanium.

The forms of $\epsilon(\vec{k})$ for electrons and holes are quite different; therefore, the calculation of the mobility tensor for each case must be treated separately. The following assumptions are made: (a) The classical Boltzmann equation is valid, with an isotropic, energy-dependent scattering time.[14] (b) Carrier scattering is due to interactions with lattice acoustic phonons. (For the temperature range from 60 to 120 °K, this has been shown to be true.[15] For carrier densities less than 4×10^{14}, carrier-carrier scattering is negligible.)[16,17] (c) Quantum effects are negligible ($\hbar\omega_c/kT<0.05$ at the maximum magnetic fields used). (d) The electrons and holes are in thermal equilibrium with the lattice due to the high carrier-lattice collision frequency. (Because the collisions are nearly elastic, the energy relaxation time is about 10^3 times the momentum relaxation time.[18] But the energy relaxation time is still less than 10^{-3} times the carrier lifetime, so the electrons and holes are in thermal equilibrium with the lattice for most of their lifetime.)

The sample orientation was chosen to be with the [111] crystal axis parallel to the magnetic field. This high-symmetry orientation was chosen to facilitate the computations of the electron- and hole-mobility tensors.

Electron-Mobility Tensor

The well-known model for the energy surface $\epsilon(\vec{k})$ of the conduction band is eight ellipsoids in the [111] crystal directions, with the effective-mass tensor diagonal in the principal coordinate system of each ellipsoid[19–21]:

$$\overleftrightarrow{M}=\begin{bmatrix} m_\perp^* & 0 & 0\\ 0 & m_\perp^* & 0\\ 0 & 0 & m_\parallel^*\end{bmatrix}.$$

Each ellipsoid is centered at the Brillouin-zone edge, so there are four equivalent ellipsoids. The Boltzmann equation is written as in Eq. (1), with the expression for the electron energy expressed in the principal coordinate system having the form

$$\epsilon(\vec{k})=\frac{h^2}{2}\left(\frac{k_x^2}{m_\perp^*}+\frac{k_y^2}{m_\perp^*}+\frac{k_z^2}{m_\parallel^*}\right).$$

The solution of this equation has been extensively discussed in the literature.[22,23] The equation is solved by putting $f=f_0+f_1$, with $f_1=-\phi(\vec{k})\partial f_0/\partial\epsilon$. Then, linearizing by taking only first-order terms in the fields gives

$$\phi(\vec{k})=\frac{-e\tau}{\hbar}\vec{\nabla}_k\epsilon\cdot\frac{\vec{F}-e\tau\overleftrightarrow{M}^{-1}\vec{F}\times\vec{B}+(e\tau)^2\vec{F}\cdot\vec{B}\overleftrightarrow{M}\vec{B}/|\overleftrightarrow{M}|}{1+(e\tau)^2\overleftrightarrow{M}\vec{B}\cdot\vec{B}/|\overleftrightarrow{M}|}\,,$$

and then the current is given by

$$\vec{j}=-e\int\vec{v}f_1\,d^3k=\frac{+e}{4\pi^3}\int\frac{\vec{\nabla}_k\epsilon}{\hbar}\,\phi(\vec{k})\frac{\partial f_0}{\partial\epsilon}\,d^3k$$

$$\equiv ne\overleftrightarrow{U}\cdot\vec{F}\,.$$

This expression defines the mobility tensor $\overleftrightarrow{U}$.

The result for the mobility expressed in the principal coordinate system of one conductivity ellipsoid is[24]

$$U_{ij}=\alpha\delta_{ij}+\beta B_iB_j(1-\delta_{ij})-\gamma\epsilon_{ijk}B_k^*\,, \quad (2)$$

where $B=(B_1,\ B_2,\ B_3)$ and $B^*=(B_1,\ B_2,\ KB_3)$, both fields being expressed in components along the principal coordinate axes of the conductivity ellipsoid; ϵ_{ijk} is the totally antisymmetric unit tensor; α, β, and γ are integrals of functions of the scattering time over the carrier-energy distribution:

$$\alpha(X)=K\mu_0^l\int_0^\infty\frac{z^2e^{-z}\,dz}{z+X}\,,$$

$$\beta(X)=\frac{9\pi}{16}K^2(\mu_0^l)^3\frac{1-\alpha(X)/K\mu_0^l}{X}\,,$$

$$\gamma(X)=\frac{3\pi}{8}K(\mu_0^l)^2\frac{2}{\sqrt{\pi}}\int_0^\infty\frac{z^{3/2}e^{-z}\,dz}{z+X}\,,$$

where

$$X=\tfrac{9}{16}\pi K(\mu_0^l)^2\vec{B}\cdot\vec{B}^*\,.$$

Here μ_0^l is the longitudinal valley mobility, and K is the ratio of longitudinal to transverse effective mass.

Now the mobility tensor for each of the four conductivity ellipsoids must be rotated from the principal coordinate system of each ellipsoid to the space axes, which are defined such that the magnetic field, parallel to the [111] crystal axis, is along the z space axis. First, the components of the magnetic field are found in the coordinate system of each ellipsoid and substituted into Eq. (2) to give the mobility tensor for each ellipsoid. Then, these tensors are individually rotated to the space axes and summed to give the final mobility tensor for the electrons. The result is

$$\overleftrightarrow{U}_n = \begin{bmatrix} \mu_\perp^n & -\mu_a^n & 0 \\ \mu_a^n & \mu_\perp^n & 0 \\ 0 & 0 & \mu_\parallel^n \end{bmatrix},$$

with

$$4\mu_\perp^n = \alpha(X_1) + \tfrac{1}{3}(5 + 4/K)\alpha(X_2) ,$$

$$4\mu_a^n = B[K\gamma(X_1) + \tfrac{1}{3}(K+8)\gamma(X_2)] ,$$

$$4\mu_\parallel^n = \alpha(X_1)/K + \tfrac{1}{3}(8 + 1/K)\alpha(X_2) + B^2[\beta(X_1) + 3\beta(X_2)] ,$$

where

$$X_1 = \tfrac{9}{16}\pi K^2(\mu_0^t)^2 B^2 ,$$

$$X_2 = \tfrac{1}{9}[\tfrac{9}{16}\pi K(\mu_0^t)^2(8+K)B^2] .$$

The integrals α, β, and γ have been tabulated, and numerical solutions for the components may be readily obtained.[25] The results are related to conductivity mobility values by requiring that $\mu_\perp^n(B=0) = \mu_c$, the conductivity mobility of electrons in germanium limited by acoustic-phonon scattering.

Hole-Mobility Tensor

The two hole bands that contribute to the conductivity are degenerate at $\vec{k}=0$; this degeneracy leads to considerable warping of the heavy-hole energy surface. For this case an analytical calculation of the mobility tensor cannot be performed; however, McClure has devised a method which allows a good approximation to the mobility to be made.[25] He considered the motion of the hole in its orbit about the magnetic field. His result is a mobility tensor whose components are expanded in harmonics of the heavy-hole rotation frequency:

$$\mu_\perp^h = \left\langle \frac{A_1\mu_c^h}{1+(\omega_c\tau)^2} + \frac{A_2\mu_c^h}{1+(2\omega_c\tau)^2} + \cdots \right\rangle ,$$

$$\mu_a^h = \left\langle \frac{A_1\omega_c\tau\mu_c^h}{1+(\omega_c\tau)^2} + \frac{A_2 2\omega_c\tau\mu_c^h}{1+(2\omega_c\tau)^2} + \cdots \right\rangle .$$

The brackets indicate averages over the hole distribution function

$$\left\langle \psi\left[\frac{\epsilon}{kT}\right]\right\rangle \equiv \frac{2}{\sqrt{\pi}}\int_0^\infty \psi(x)e^{-x}x^{3/2}dx .$$

The amplitudes of the harmonics depend on the form of the energy surface and are not readily calculable for a general surface; however, it is possible, using knowledge of the crystal symmetry, to derive maximum amplitudes for the harmonics. For the case of the magnetic field along the [001] crystal axis, giving fourfold symmetry about the magnetic field, this has been done and the results compared with experiment. The coefficients necessary to fit experiment to theory were found to lie between the maximum amplitudes and those for a spherical energy surface.[26] For our orientation there is threefold symmetry about the magnetic field. For this case the maximum values of the harmonics are

$$A_1 = 1 , \quad A_3 = 0 ,$$

$$A_2 = \tfrac{1}{4} , \quad A_4 = \tfrac{1}{16} .$$

The terms A_i for $i > 2$ will have little effect; at $\omega_c\tau = 1$, the fourth term in $\mu_\perp^h$ is less than 1% of the first. Therefore, we include only A_1 and A_2 in the hole mobility. We choose $A_1 = 1$ and $A_2 = 0.15$, between the limits calculated for the spherical energy surface and the triangular one. We also need a relationship between $\omega_c\tau$ and $\mu_c^h B$. For the case of cubic energy surfaces, it was found experimentally that $\omega_c\tau = 0.94\mu_c^h B$. We arbitrarily use this result in our numerical evaluation of the hole mobility. These two choices do not strongly affect the theoretical predictions. They essentially affect only slightly the scaling of the mobility, and they leave the form of the $D_\perp(B)$ prediction unchanged.

The final expressions for the heavy-hole mobility-tensor components are

$$\mu_\perp^h = (\mu_c^h/1.15K\mu_0^t)[\alpha(\nu_1) + 0.15\alpha(\nu_2)] ,$$

$$\mu_a^h = [(\mu_c^h)^2 B/0.70K(\mu_0^t)^2][\gamma(\nu_1) - 0.3\gamma(\nu_2)] ,$$

where

$$\nu_1 = \tfrac{9}{16}\pi(0.94\mu_c^h B)^2 ,$$

$$\nu_2 = \tfrac{9}{16}\pi(1.88\mu_c^h B)^2 ,$$

and α and γ are defined above.

This theory is unable to provide an expression of hole mobility parallel to the magnetic field; for this component we shall use results experimentally obtained.

The light-hole band contains about 4% of the holes. It is known to have a nearly spherical energy surface, with a mobility eight times that of the heavy-hole conductivity value.[27] The mobility tensor for this band may be written

$$\overleftrightarrow{U}^l = \begin{bmatrix} \dfrac{\mu^l}{1+(\mu^l B)^2} & \dfrac{(\mu^l)^2 B}{1+(\mu^l B)^2} & 0 \\ -\dfrac{(\mu^l)^2 B}{1+(\mu^l B)^2} & \dfrac{\mu^l}{1+(\mu^l B)^2} & 0 \\ 0 & 0 & \mu^l \end{bmatrix} .$$

Absolute values of electron and total hole conductivity mobilities are taken to be equal, as has been found by Morin for the temperature range in which we are working.[15] The values for μ_c^h and μ^l are found by setting the total hole conductivity mobility $0.96\mu_c^h + 0.04\mu_c^l$ equal to the electron conductivity mobility, and noting that $\mu^l = 8\mu_c^h$.

Dependence of Diffusion Coefficients on Magnetic Field

The solution of the equations of motion for the holes and electrons has been found in terms of a mobility tensor for each species. Combination of these results with the continuity equation will allow us to solve for the plasma diffusion coefficient as a function of the magnetic field. For each calculation below we assume that the diffusion is ambipolar, so the particle fluxes in the direction of the density gradient may be set equal. This allows us to solve for the ambipolar electric field, which is the only electric field assumed to exist in the crystal. As the material is n type at liquid-nitrogen temperatures, we set N equal to the number of extrinsic electrons, and neglect the very small number of extrinsic holes. Three cases will be considered: (i) diffusion parallel to the magnetic field in a rectangular geometry, (ii) diffusion perpendicular to the magnetic field in a rectangular geometry, and (iii) diffusion perpendicular to the magnetic field in a cylindrical geometry. The calculations are similar for the three cases. The case of perpendicular diffusion in the rectangular geometry will be shown in some detail; only the resultant differential equations will be presented for the other two cases.

Perpendicular Diffusion, Rectangular Geometry

Using the equations of motion as derived above, we may write expressions for the hole and electron fluxes into the sample:

$$\Gamma_n = -n\mu_\perp^n E_a - \frac{kT}{e}\mu_\perp^n \frac{\partial n}{\partial y}\,,$$
$$\Gamma_p = p^l \mu_\perp^l E_a - \frac{kT}{e}\mu_\perp^l \frac{\partial p^l}{\partial y} + p^h \mu_\perp^h E_a - \frac{kT}{e}\mu_\perp^h \frac{\partial p^h}{\partial y}\,. \tag{3}$$

These expressions may be considerably simplified by noting that the light and heavy holes are always in equilibrium with each other, with $p^h = 0.96p$ and $p^l = 0.04p$. Then we can make the abbreviation $p^l\mu_\perp^l + p^h\mu_\perp^h = pu_\perp^p$, giving $\mu_\perp^p = 0.96\mu_\perp^h + 0.04\mu_\perp^l$, and Eq. (3) takes the form

$$\Gamma_p = pu_\perp^p E_a - \frac{kT}{e}\mu_\perp^p \frac{\partial p}{\partial y}\,.$$

The continuity equation for electrons, for example, is

$$\frac{\partial n}{\partial t} + \vec{\nabla}\cdot\vec{\Gamma}_n = -\frac{n}{\tau_n}\,.$$

With the assumptions of quasineutrality and that $\tau_n = \tau_p$, it is readily apparent that $\vec{\Gamma}_n = \vec{\Gamma}_p$. From experimental results to be presented below, we have found that τ does not depend on the injected plasma density. This result is expected for low trap densities ($N_t < N$) and high injected carrier densities ($n > N$). Then under these conditions $n_{inj} = P_{inj}$ and $\tau_n = \tau_p$.[28] Setting the fluxes of holes and electrons equal allows us to solve for the ambipolar electric field:

$$E_a = \frac{kT}{e}\,\frac{\mu_\perp^p \partial p/\partial y - \mu_\perp^n \partial n/\partial y}{p\mu_\perp^p + n\mu_\perp^n}\,.$$

Then, using this expression in the electron equation of motion allows us to write the electron flux into the sample in terms of the electron density gradient:

$$\Gamma_n = -\frac{kT}{e}\,\frac{\mu_\perp^n \mu_\perp^p (n\partial p/\partial y + p\partial n/\partial y)}{p\mu_\perp^p + n\mu_\perp^n}\,.$$

Inserting this result into the continuity equation gives a differential equation for the plasma density as a function of position into the sample:

$$\frac{n}{\tau_r} = \frac{kT}{e}\mu_\perp^n \mu_\perp^p \frac{\partial}{\partial y}\,\frac{n\partial p/\partial y + p\partial n/\partial y}{p\mu_\perp^p + n\mu_\perp^n}\,.$$

The result is simplified by writing $n = n_{inj} + N$ and $p = p_{inj} = n_{inj}$:

$$\frac{n_{inj}}{L^2} = \frac{\partial^2 n_{inj}}{\partial y^2}\left(1 - \frac{\delta N'}{n_{inj} + N'}\right) + \left(\frac{\partial n_{inj}}{\partial y}\right)^2 \frac{\delta N'}{(n_{inj} + N')^2}\,, \tag{4}$$

where

$$\delta = \frac{\mu_\perp^n - \mu_\perp^p}{2\mu_\perp^n} \ll 1\,, \quad N' = \frac{N\mu_\perp^n}{\mu_\perp^n + \mu_\perp^p}\,,$$
$$L^2 = \frac{2\mu_\perp^n \mu_\perp^p kT\tau_r}{e(\mu_\perp^n + \mu_\perp^p)} = D_\perp \tau_r\,. \tag{5}$$

The δ term results from the fact that for our large injected plasma density the ambipolar diffusion coefficient is dependent on the density. The solution to first order in δ, taking dominant terms in $N'/n_{inj} < 1$, is

$$n_{inj}(y) = n(0)e^{-y/L}\left[1 - \frac{\delta}{2}\left(\frac{N'}{n_{inj}}\right)^2 \frac{y}{L} + \cdots\right]\,.$$

The dominant term is the familiar exponential decay of density with distance into the sample, with decay length given by $L = (D_\perp \tau_r)^{1/2}$. For our experimental conditions $\delta < 0.2$ for $\mu B < 6$, $N'/n_{inj} < 0.2$, and $y/L < 2$, so the maximum correction due to the extrinsic electron density is less than 1%, and may be neglected.

Parallel Diffusion, Rectangular Geometry

The solution for the plasma-density distribution in

this case is identical to that treated above but for the replacement of μ_1^n by $\mu_{\parallel}^n$ and μ_1^p by $\mu_{\parallel}^p$ in Eq. (4). The expression for the diffusion length then becomes

$$L^2 = \frac{2\mu_{\parallel}^n \mu_{\parallel}^p kT\tau_r}{e(\mu_{\parallel}^n + \mu_{\parallel}^p)} \quad . \tag{6}$$

This expression is evaluated using the theoretically derived values for $\mu_{\parallel}^n$ and the experimentally obtained values for $\mu_{\parallel}^p$ from Furth and Waniek.[29]

Perpendicular Diffusion, Cylindrical Geometry

Solving for the ambipolar electric field and using that result in the electron continuity equation gives the following differential equation to be solved for the plasma-density distribution:

$$\frac{n_{inj}}{L^2} = \left(\frac{\partial^2 n_{inj}}{\partial r^2} + \frac{1}{r}\frac{\partial n_{inj}}{\partial r}\right)\left(1 - \frac{\delta N'}{n_{inj} + N'}\right) + \frac{\partial n_{inj}}{\partial r}\frac{\delta N'}{(n_{inj} + N')^2} \quad ,$$

where L is given by Eq. (5).

The solution for $\delta = 0$ is the Bessel function K_0, which may be approximated to within 2% by $K_0 = Lr^{-1/2}e^{-r/L}$. Then, to first order in δ we find

$$n(r) = n_0\left(\frac{r}{L}\right)^{-1/2} e^{-r/L}\left[1 - \frac{\delta}{4}\left(\frac{N'}{n_{inj}}\right)^2 \frac{r}{L} + \cdots\right] \quad .$$

Because the injected plasma in the cylindrical case was less than in the rectangular case the term due to the extrinsic electron density is larger; however, its maximum size for our experimental conditions is less than 10% of the dominant term, and again the correction will be neglected.

III. EXPERIMENT

Sample Preparation

The material used in these experiments was n-type single-crystal germanium obtained from Sylvania Electronic Products. The extrinsic electron density was 3×10^{12} cm^{-3} at 85 °K. The samples were obtained by x-ray diffraction techniques to have one face within 4° of the [111] crystal axis. This axis was always kept parallel to the magnetic field. The two facing sides which were to serve as infrared windows were lapped with progressively finer grades of lapping compound, finishing with 0.3-μ particle size. They were lapped at an angle of $\frac{1}{2}$ degree with respect to each other to eliminate Fabry-Perot effects. The surface that was to be the one at which the plasma was injected was lapped with 1-μ lapping compound and then etched in CP4A[30] for 45 sec to remove damaged material remaining from the lapping operation. Because of the difficulty of lapping the hole in the cylindrical sample, it was etched for 150 sec to ensure that all damaged material was removed. Then the samples were washed in distilled water and etched in[31] Ge No. 5 to give the final low surface-recombination surface.[32] This completed the preparation of the cylindrical and rectangular samples used for measurement of diffusion parallel to the magnetic field. The rectangular sample, used for measurement of diffusion perpendicular to the magnetic field, had four voltage probes of 2-mil gold wire welded to the plasma injection surface about 1.5 mm apart, in a row in the direction of the diamagnetic current. The function of these probes will be described later. Two current leads were connected to the ends of the sample, using silver-filled epoxy. The rectangular samples were $10\times10\times5$ mm in the direction of plasma diffusion. The cylindrical sample was 25 mm o.d. by 10 mm i.d. by 10 mm thick.

Plasma Injection Source

The plasma source was a high-pressure 500-W mercury arc. The light was collimated by an $f/1.2$ Pyrex lens and passed through a rotating chopper, which modulated it at 105 Hz. The light from the chopper was passed through a 1-cm water filter and a second Pyrex lens, which focussed it near the sample. The water filter removed all light with wavelength greater than 1.4 μ; the remaining light was strongly absorbed by the germanium at its surface. This filtering ensures that all plasma inside the sample is there due to diffusion from the surface and not because of volume generation by weakly absorbed light. The carriers, which were excited by light with wavelengths shorter than the band edge, had an energy higher than the lattice temperature, but they quickly relaxed to the lattice temperature due to collisions with acoustic and optical phonons.[18] For the rectangular samples, the plasma-injection light was measured to be uniform within ±2% over the injection surface, by using a calibrated germanium photoconductor. The maximum injected plasma density was 2×10^{14} cm^{-3}. For the cylindrical sample, the plasma-injection light was measured to be uniform to within ±4% in the azimuthal direction. This was accomplished using a second cylindrical sample to which a photovoltaic probe was attached on the illuminated surface. The photovoltage was calibrated, as a function of illumination, with calibrated screens. Rotation of the detector sample in the sample mount allowed measurement of the azimuthal variation of the injection light. The maximum plasma density in the cylindrical sample was 1.5×10^{13} cm^{-3}.

Plasma-Density Measurement

The plasma-density measurement was based on the fact that the absorption of infrared radiation of wavelength greater than the band edge, passing through germanium, is dependent on the number

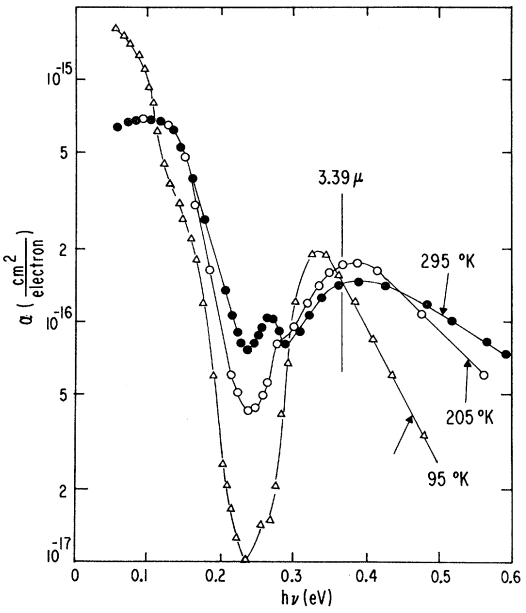

FIG. 1. Experimentally measured absorption coefficient of infrared radiation in germanium (see Ref. 31).

of free electrons and/or holes present. The absorption coefficient is shown in Fig. 1 as a function of temperature and wavelength.[33] The peak at about 0.35 eV is caused by transitions between the spin-orbit splitoff hole band and the remaining two hole bands. The absorption peak has been shown to be independent of the type and number of acceptor atoms, and to be proportional to the density of free holes.[34] The proportionality has been shown to hold for nonequilibrium injected holes, as well as for those in thermal equilibrium.[35] Therefore, absorption of infrared radiation at 0.35 eV is ideally suited for our application as a plasma-density probe.

A helium-neon laser was used as a source of infrared radiation at 3.39 μ, very close to the absorption peak. A 1-in. focal-length quartz lens was used to focus the beam onto the sample, and a similar lens was used to collimate the emerging beam. The beam diameter (at half-power points) was measured to be 0.11 mm at the sample position, which is close to the diffraction-limited value of 0.07 mm. For an exponential decay of plasma density with distance, resolution is limited by the precision of the mechanical system moving the laser beam across the plasma profile, and not by the size of the laser beam, as long as the beam is entirely within the plasma.

Access to the sample in the magnet was perpendicular to the magnetic field. For measurement of diffusion parallel to the magnetic field, the infrared beam was directed through the sample perpendicular to the field. The Dewar had two quartz windows. The lenses and detector were mounted on a bar that was moved with a micrometer screw across the magnetic field to sample the plasma density, the sample remaining fixed. Figure 2 is a sketch of the apparatus used for measurement of plasma diffusion parallel to the magnetic field.

For measurement of diffusion perpendicular to the magnetic field it was necessary to direct the laser beam parallel to the field. Two quartz prisms were mounted on the Dewar tailpiece, to divert the beam so that it traversed the sample parallel to the magnetic field. The lenses were also fixed to the tailpiece. The plasma was scanned by moving the sample vertically across the stationary laser beam. A sketch of the apparatus used for measurement of diffusion in the rectangular sample perpendicular to the magnetic field is shown in Fig. 3. The only difference between the rectangular-sample arrangement and that used for the cylindrical sample is in the method of injecting the plasma. The plasma-injection scheme used for the cylindrical sample is shown in Fig. 4.

After having traversed the sample, the laser beam was directed onto a room-temperature lead-sulphide infrared detector obtained from Santa Barbara Research Corporation. The resulting signal was measured with a PAR HR 8 lock-in amplifier, which was synchronized to the frequency

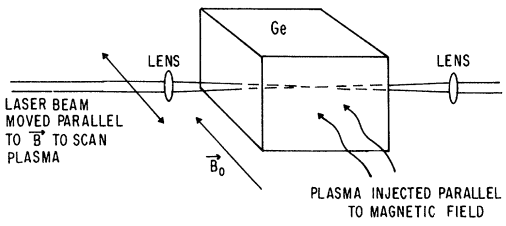

FIG. 2. Pictorial representation of the optical apparatus for the measurement of diffusion parallel to the magnetic field.

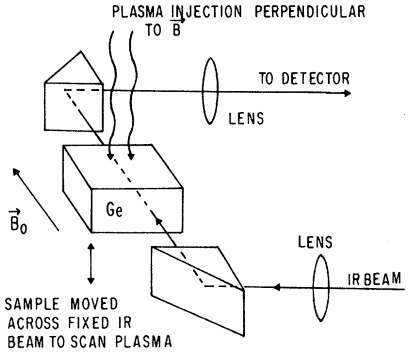

FIG. 3. Pictorial representation of the optical apparatus for the measurement of diffusion perpendicular to the magnetic field.

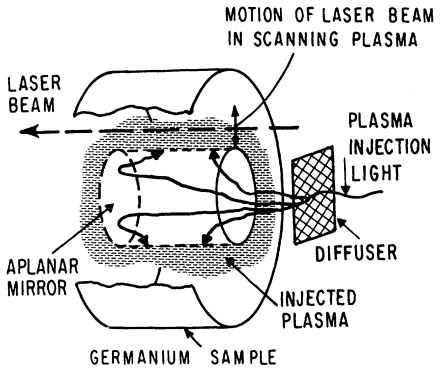

FIG. 4. Plasma-injection method for cylindrical sample. The combination of diffuser and aplanar mirror gives uniform injection on the interior of the hole through the sample.

of the plasma-injection light chopper. Figure 5 is a schematic diagram of the entire plasma generation and measurement apparatus.

The lower limit on measurable plasma density was determined by the noise resulting from mechanical vibration. The minimum measurable signal was $\Delta I/I_0 = 5\times10^{-4}$, corresponding to a plasma density of 3×10^{12} cm^{-3}. The noise that limited this sensitivity was carried on the laser beam, so increasing the laser power did not improve the sensitivity.

The experimental results were collected in the following manner. The magnetic field was set at a fixed value. For perpendicular diffusion in the rectangular sample, an external current source was used to set the diamagnetic current so that the voltage in the diamagnetic direction, measured by the four probes on the sample surface, was zero. This procedure was necessary to overcome contact resistance. This procedure was unnecessary for the cylindrical sample, since the diamagnetic current flowed entirely within the sample. Each sample was moved vertically across the laser beam in increments of $\frac{1}{8}$ mm. At each point the total transmitted laser beam intensity, and the modulation on the beam due to absorption by the injected plasma, were measured. The absorption of the laser beam was directly proportional to the plasma density. Such measurements of plasma density (as a function of distance) for the rectangular sample are shown in Fig. 6. They may be fitted with a straight line to give the diffusion length.

IV. EXPERIMENTAL RESULTS AND DISCUSSION

The experimental data for the case of diffusion parallel to the magnetic field are shown in Fig. 7. There is good agreement with the theory [Eq. (6)] for all magnetic fields. The value of conductivity mobility used to scale the theoretical curve is 2.8 m^2/V sec, in good agreement with other measurements in the literature.[13] In gaseous plasmas one does not find that the diffusion coefficient parallel to the magnetic field is affected by the magnetic

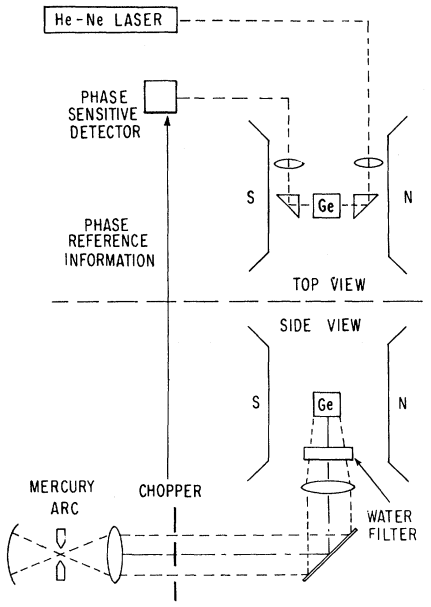

FIG. 5. Schematic diagram of the infrared density probe and plasma-injection apparatus.

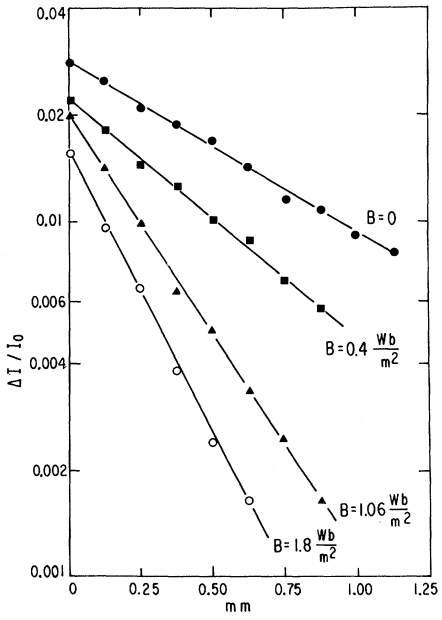

FIG. 6. Laser measurements of plasma density in germanium as a function of position in germanium crystal, for diffusion perpendicular to the magnetic field, with magnetic field as parameter.

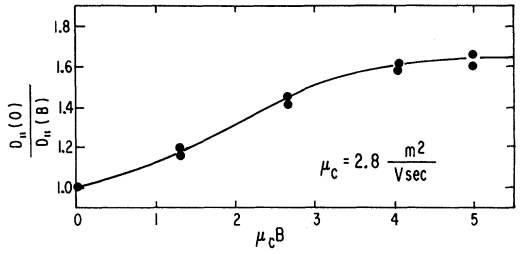

FIG. 7. Measured variation of parallel diffusion coefficient in germanium with magnetic field (dots) and theory (solid line) for sample at a temperature of 88 °K.

field. However, in this solid-state plasma, interaction of the carriers with the lattice gives rise to this unusual effect.

The good agreement between theory and experiment, for all values of magnetic field, shows that the recombination lifetime is unaffected by the magnetic field. This fact is important in the discussion of the perpendicular diffusion results.

For both the parallel and perpendicular diffusion measurements, the variation of plasma density with distance into the sample is exponential. This fact shows that the recombination is correctly described in the theory by a one-body recombination term, even for injected carrier densities much larger than the extrinsic carrier density. This result is expected for certain densities of recombination centers in germanium.[28]

The experimental results for the case of diffusion perpendicular to the magnetic field are shown in Fig. 8 for the rectangular geometry and in Fig. 9 for the cylindrical geometry. The value of conductivity mobility, $\mu_c = 2.8\ m^2/V\,sec$, for the theoretical curves [Eq. (5)] is chosen so that the theoretical curve fits the experimental points for low magnetic fields. This value of mobility agrees well with that determined by others for this temperature.[13] There is more scatter in the results for the cylindrical geometry because of difficulties in measuring the lower injected plasma density. Nevertheless, these results show the same trend as those for the rectangular geometry. The fit of theory to experimental results is good for $\mu_c B < 3.5$, but for larger values of $\mu_c B$ the experimentally determined diffusion coefficient does not decrease as rapidly as predicted with increasing magnetic field. Following Geissler, we write $D = D_{\text{theory}} + D_{\text{excess}}$, where D_{excess} represents the unexplained or "anomalous" diffusion. We observe that D_{excess} is negligibly small at low magnetic fields, but at the highest achievable values of $\mu_c B$, D_{excess} reaches a value of about 1.5 times the Bohm value $\frac{1}{16} kT/eB\ cm^2sec^{-1}$.

The large scatter in our measurement of $D_\perp(0)/$

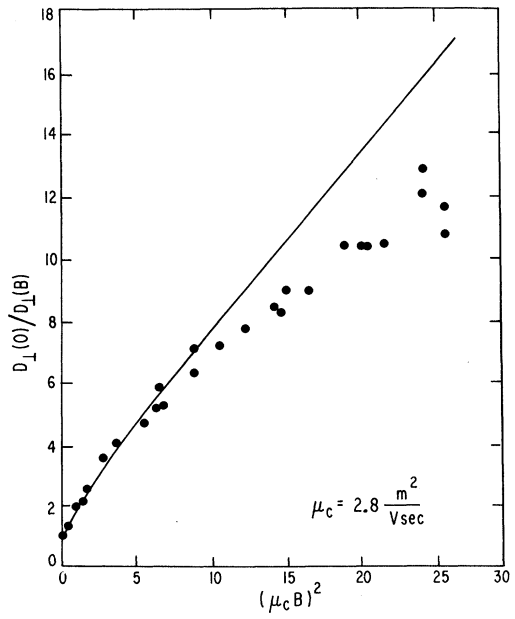

FIG. 8. Measured variation of perpendicular diffusion coefficient in germanium with magnetic field (dots) and theory (solid line) for rectangular sample at a temperature of 92 °K. The difference at high magnetic fields is of the order of the Bohm diffusion coefficient. The scatter of the experimental points is indicative of the experimental reproducibility.

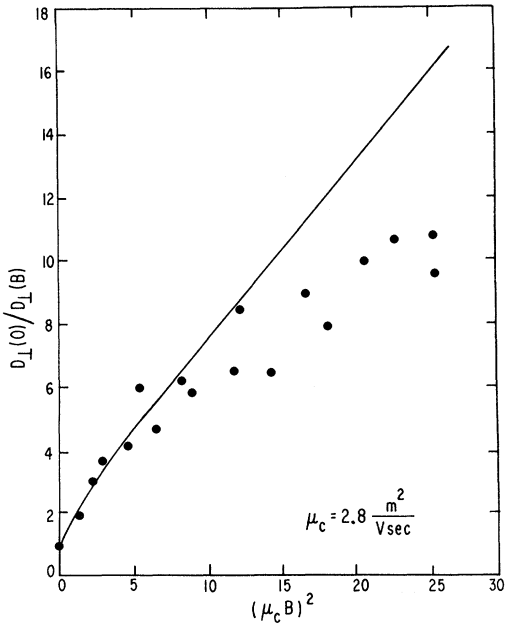

FIG. 9. Measured variation of perpendicular diffusion coefficient in germanium with magnetic field (dots) and theory (solid line) for cylindrical sample at a temperature of 95 °K. The difference at high magnetic fields is of the order of the Bohm diffusion coefficient. The scatter of the experimental points is indicative of the experimental reproducibility.

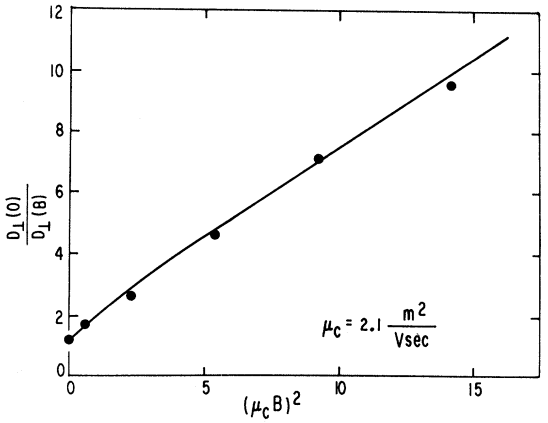

FIG. 10. Measured variation of perpendicular diffusion coefficient in germanium with magnetic field (dots) and theory (solid line) for rectangular sample at a temperature of 111 °K.

$D_\perp(B)$ in Figs. 8 and 9 is probably due to the method of presenting the results. The experimentally measured quantity is the diffusion length L, which is related to $D_\perp(0)/D_\perp(B)$ by

$$D_\perp(0)/D_\perp(B) \propto 1/L^2 .$$

Then the scatter is

$$\Delta\left(\frac{D_\perp(0)}{D_\perp(B)}\right) \propto \frac{-2}{L^2}\,\frac{\Delta L}{L} .$$

So for a fixed relative scatter $\Delta L/L$ in L, at large magnetic fields where L is small, the scatter in the values of $D_\perp(0)/D_\perp(B)$ is expected to be greater than that at low magnetic fields.

The method of laser-beam absorption measurement, which utilized lock-in detection and integration over several hundred plasma-injection pulses, tended to average out any plasma fluctuations. Therefore it is very unlikely that the scatter in $D_\perp(0)/D_\perp(B)$ at large magnetic fields is due to plasma turbulence effects.

Experimental results for the case of lower carrier mobility, obtained by heating the rectangular sample to 111 °K, are shown in Fig. 10. These results agree with the theory [Eq. (4)] for all magnetic fields, so the enhanced diffusion is not determined by magnetic field alone, but is also dependent on the scattering time τ.

There is nothing in our results which would indicate a reason for the enhanced diffusion. It is known that dc electric fields have been the cause of enhanced diffusion in multipole and Q-plasma devices. We had suspected that possible problems associated with the current contacts in the rectangular geometry could be the cause of dc electric fields which would affect the diffusion, but the contactless cylindrical sample gave identical results.

Often in gaseous plasmas enhanced diffusion is accompanied by oscillations in the plasma. The voltage probes on the rectangular sample were used to look for oscillations in the plasma. No oscillations were seen over a frequency range from 200 Hz to 20 MHz, using detectors with a minimum sensitivity of $0.001kT$ V. It is possible that oscillations outside of the frequency range studied were present, or that they did not couple to the probes.

It is interesting to compare the present results with those obtained by Moore and Kessler in their measurements of the magnetic moment of a solid-state plasma.[36] They measured the diamagnetic current associated with the diffusion of the plasma to the surface of the crystal, and used a single-particle theory that did not include anisotropic effects to describe the plasma motion. For values of $\omega_c\tau < 1$, they had agreement with their theory, but for $\omega_c\tau > 1$, the experimental results diverged from the theory. We find that our anisotropic theory also fails to agree with their experimental results. They attributed the deviation of experiment from theory to effects of the nonuniform magnetic field. It is also possible that an enhanced diffusion would cause the diamagnetic current to differ from that predicted.

In connection with our measurements of the diffusion length of the electron-hole plasma we also made measurements of the PEM short-circuit current. We found that the exact form of the current dependence on magnetic field differed from sample to sample, depending critically on the surface treatment. This is expected from theoretical analysis. However, we noted that a good fit between theory and experiment, for the variation of the PEM current with magnetic field, could always be obtained by choosing an appropriate value for the surface-recombination coefficient. This result is surprising, since we found that the theory was inadequate to describe the diffusion effects at large values of $\omega_c\tau$. It turns out that varying the surface-recombination coefficient in the theory mainly affects the form of the PEM current for large magnetic fields. Therefore, choosing an incorrect value of the surface-recombination coefficient can cancel out the effect of the enhanced diffusion on the PEM currents. Thus, the inadequancy of the present theory to describe the diffusion of an electron-hole plasma in germanium does not become apparent in analysis of PEM measurements, for which there is a free parameter available to adjust the form of the theoretical predictions.

Several directions are possible for extending the present results. Among them would be the desirable one of extending the measurements to higher values of $\omega_c\tau$, either by using larger values of magnetic field, or by going to lower temperatures, or both. These measurements would make it possible to determine the magnetic-field dependence of the enhanced diffusion. Also, a more thorough search

for oscillations might give an indication of the mechanism involved.

ACKNOWLEDGMENTS

The authors wish to thank M. Glickman for several very helpful discussions. Special thanks for machining and technical assistance are due to R. W. Yager, H. H. Higgins, and L. Pursell. The crystal face orientation was accomplished by R. T. Smith of RCA Sarnoff Laboratories.

†Work supported jointly by U. S. Atomic Energy Commission under Contract No. AT(30-1)-1238 and by the National Aeronautics and Space Administration.

[1]T. Dodo, Institüt für Plasmaphysik Report No. 2/62, 1967 (unpublished).
[2]K. H. Geissler, Phys. Rev. 171, 179 (1968).
[3]B. J. Eastlund, K. Josephy, R. Leheny, and T. Marshall, Phys. Fluids 9, 2400 (1966).
[4]D. Bohm, E. H. S. Burhop, and H. S. W. Massey, in *Characteristics of Electrical Discharges in Magnetic Fields*, edited by A. Guthrie and R. K. Wakerling (McGraw-Hill, New York, 1949), p. 13.
[5]E. Hinnov and A. S. Bishop, Phys. Fluids 9, 195 (1966).
[6]D. L. Jassby and R. W. Motley, Phys. Fluids 12, 258 (1969).
[7]B. Ancker-Johnson and J. E. Drummond, Phys. Rev. 132, 2372 (1963).
[8]N. J. Harrick, Phys. Rev. 103, 1173 (1954).
[9]B. Ancker-Johnson, in *Proceedings of the International Symposium on Plasma Effects in Solids* (Dunod, Paris, 1964), p. 165.
[10]R. E. Slusher, W. Giriat, and S. R. J. Brueck, Phys. Rev. 183, 758 (1969).
[11]S. W. Kurnick and R. N. Zitter, J. Appl. Phys. 27, 278 (1956).
[12]W. Gartner, Phys. Rev. 105, 823 (1956).
[13]L. L. Campbell, *Galvanomagnetic and Thermomagnetic Effects: The Hall and Allied Phenomena* (Longmans Green, New York, 1923), p. 125.
[14]R. A. Smith, *Semiconductors* (Cambridge U.P., London, 1961), p. 289.
[15]F. J. Morin, Phys. Rev. 93, 62 (1954).
[16]J. Appel and R. Bray, Phys. Rev. 127, 1603 (1962).
[17]D. M. Brown and R. Bray, Phys. Rev. 127, 1593 (1962).
[18]M. A. Habegger and H. Y. Fan, Phys. Rev. Letters 12, 99 (1964).
[19]B. Abeles and S. Meiboom, Phys. Rev. 93, 1121 (1954); 95, 31 (1954).
[20]B. Lax, H. J. Zeiger, R. N. Dexter, and E. S. Rosenblum, Phys. Rev. 93, 1418 (1954).
[21]M. Shibuya, Phys. Rev. 95, 1385 (1954).
[22]H. Y. Fan, *Solid State Physics* (Academic, New York, 1955), Vol. I, p. 283.
[23]H. Jones, Proc. Roy. Soc. (London) A155, 653 (1936).
[24]A. C. Beer, *Solid State Physics* (Academic, New York, 1963), Vol. IV, p. 199.
[25]J. W. McClure, Phys. Rev. 101, 1642 (1956).
[26]C. Goldberg, E. N. Adams, and R. E. Davis, Phys. Rev. 105, 865 (1957).
[27]R. Willardson, T. Harman, and A. Beer, Phys. Rev. 96, 1512 (1954).
[28]J. S. Blakemore, *Semiconductor Statistics* (Pergammon, New York, 1962), p. 282.
[29]H. P. Furth and R. W. Waniek, Phys. Rev. 104, 343 (1956).
[30]CP4A: 25 ml HNO_3, 15 ml HF.
[31]Ge No. 5: 40 ml HF, 6 ml 30% H_2O_2, 24 ml distilled water.
[32]S. G. Ellis, J. Appl. Phys. 28, 1262 (1957).
[33]W. E. Pinson and R. Bray, Phys. Rev. 136, A1449 (1964).
[34]W. Kaiser, R. J. Collins, and H.Y. Fan, Phys. Rev. 91, 1380 (1953).
[35]H. B. Briggs and R. C. Fletcher, Phys. Rev. 91, 1342 (1953).
[36]A. R. Moore and J. O. Kessler, Phys. Rev. 132, 1494 (1963).

PHYSICAL REVIEW A VOLUME 5, NUMBER 1 JANUARY 1972

Photoionization Cross Section of the Neutral Iron Atom*

Hugh P. Kelly and Akiva Ron†
Department of Physics, University of Virginia, Charlottesville, Virginia 22901
(Received 31 March 1971)

Calculations are presented for the photoionization cross section of the neutral iron atom for photon energies from threshold to 10 keV. Our results are based upon the use of nonrelativistic wave functions and the dipole approximation. Correlations are included to low orders by the use of many-body perturbation theory; and the cross section including correlations is found to differ greatly from that obtained from the Hartree-Fock approximation. Hartree-Fock results are also presented for comparison. We roughly estimate our cross section, including correlations near threshold, to be accurate to within a factor of 2 when integrated over a few eV.

I. INTRODUCTION

Photoionization cross sections are of considerable interest in atomic physics and in astrophysics, and it is desirable to have reliable cross sections over a wide range of energy for many elements. Excel-